Capillary Microfluidics-Assembled Virus-like Particle Bionanoreceptor Interfaces for Label-Free Biosensing
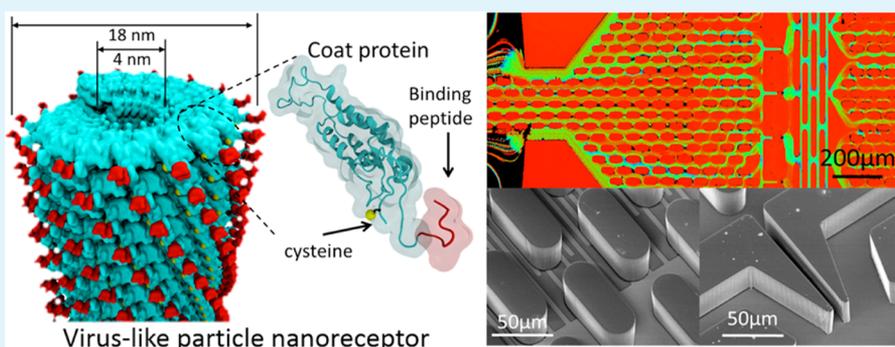
Faheng Zang,[†,∥] Konstantinos Gerasopoulos,[†] Adam D. Brown,[‡,§] James N. Culver,[§,⊥] and Reza Ghodssi*,[†]

[†]Department of Electrical and Computer Engineering, Institute for Systems Research, [‡]Fischell Department of Bioengineering, [§]Institute for Bioscience and Biotechnology Research, and [⊥]Department of Plant Science and Landscape Architecture, University of Maryland, College Park, Maryland 20740, United States
[∥]Department of Electrical Engineering, Princeton University, Princeton, New Jersey 08544, United States

S *Supporting Information*

ABSTRACT: A capillary microfluidics-integrated sensor system is developed for rapid assembly of bionanoreceptor interfaces on-chip and label-free biosensing. Genetically engineered *Tobacco mosaic virus* (TMV) virus-like particles (VLPs), displaying thousands copies of identical receptor peptides FLAG-tags, are utilized as nanoceptors for antibody sensing. Controlled and accelerated assembly of VLP receptor layer on impedance sensor has been achieved using capillary action and surface evaporation from an open-channel capillary microfluidic system. VLPs create a dense and localized receptor monolayer on the impedance sensor using only 5 μL of VLP sample solution (0.2 mg/mL) in only 6 min at room temperature. The VLP-functionalized impedance sensor is capable of label-free detection of target antibodies down to 55 pM concentration within 5 min. These results highlight the significant potentials of an integrated microsystem for rapid and controlled receptor–transducer interface creation and the nanoscale VLP-based sensors for fast, accurate, and decentralized pathogen detection.

KEYWORDS: *nanoreceptor, virus-like particle, capillary microfluidics, label-free, biosensor*

INTRODUCTION

Outbreaks of contagious diseases caused by viral and bacterial infections have escalated due to rapid mutation of pathogen and the convenience of global transportation.[1−3] In order to contain the spread of diseases at early stages, diagnostic technologies need to be adapted and further developed to achieve reduced response times and improved accuracy. One direction in the effort toward rapid diagnoses is to perform decentralized (point-of-care) pathogen detection and disease control[4,5] using miniaturized biosensors. Biosensors are analytical devices that utilize the integration of biological sensing receptors with physical sensors. Their transduction mechanisms convert biological target molecule binding events into measurable electrical signals to quantify target molecule concentration.[6] Miniaturized biosensors are increasingly implemented in point-of-care pathogen detection due to their extraordinary portability, versatility, and low cost.[7−9] They provide fast and reliable alternatives to central analytical facilities. One challenge associated with biosensor miniaturization is achieving high receptor density while maintaining a limited footprint, ensuring both sufficient sensitivity and a low device profile. To address this challenge, biological receptors such as peptides, antibodies, enzymes, aptamers, and cells with inherent biodetection selectivity have been integrated into sensors through microfabrication processes.[10,11] However, low receptor density and complex surface chemistry in the immobilization of receptors on transducers are common bottlenecks in biosensor development, adding to the cost, complexity, and time for sensor preparation. Meanwhile, fluctuations in the environmental conditions during conventional microfabrication processes also affect the stability of bioreceptors. Therefore, new sensing receptors and sensor
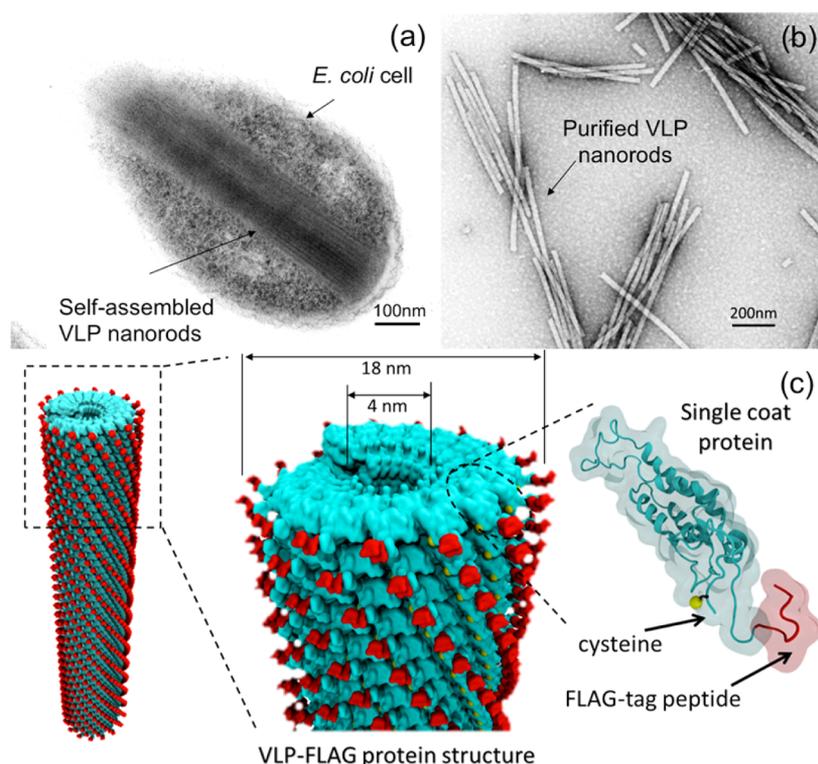
Figure 1. Transmission electron microscopy (TEM) images of (a) VLP nanorods formed in an *E. coli* bacterial cell and (b) VLP nanorods after purification from the cell residues. (c) Three-dimensional schematics of a VLP formed by helical arrangements of identical CPs expressing cysteine residues and FLAG-tag sequences.

functionalization protocols that can simultaneously simplify sensor preparation and maximize sensor performance are desired for next generation portable biosensors.

In nature, macromolecules offer a rich library of new sensing receptors with enormous variety in their structures and properties to address the aforementioned challenges.[12−16] Particularly, the *Tobacco mosaic virus* (TMV) virus-like particle (VLP), one of the emerging biological macromolecules comprising both nanoscale structures and biorecognition elements, is a superb candidate for bionanoreceptors in portable biosensors. A wide variety of programmable receptor peptides can be genetically expressed on the thousands of identical coat proteins (CPs) on a single TMV VLP surface, yielding extremely high receptor density at the molecular level.[17−19] Meanwhile, surface-attachment-promoting cysteine residues can also be engineered into the CP genetic code, facilitating self-assembly of VLPs on device surfaces without any additional chemical surface modifications.[20,21] Previously, TMV VLPs have been successfully demonstrated as receptors in impedimetric and electrochemical sensors for biological or chemical detection.[22−24] However, challenges such as long VLP self-assembly time (3−18 h) and low VLP assembly density restrain the performance of VLP-based biosensors.

This work utilizes microsystem solutions to integrate VLP bionanoreceptors, capillary microfluidics, and impedimetric microsensors for rapid sensor functionalization and enhanced biosensing. As a model system for biomolecular detection, a VLP construct genetically modified with a C-terminal FLAG-tag peptide sequence and an N-terminal cysteine residue is implemented as the nanoreceptor (VLP-FLAG), and anti-FLAG IgG serves as the target molecule. The binding event between the VLP-FLAG bionanoreceptor and the target antibody is studied as a model system to understand the performance of the VLP-functionalized sensor.

■ MATERIALS AND METHODS

Genetically Engineered TMV VLPs as Bionanoreceptors. The VLP-FLAG nanoreceptors are self-assembled from TMV CPs that have been genetically modified to assemble into nanoscale rods, like wild-type TMV, but without the genomic RNA (genetic modifications are detailed in the Supporting Information). They are thereby inherit the high surface-to-volume ratio and helically arranged structures of TMVs while being noninfectious. This indicates that VLP can carry 2130 identical CP units in a nanorod structure with 18 nm in diameter and 300 nm in length. The VLP CP was expressed in a bacterial expression system and self-assembled into rodlike structures hundreds of nanometers long containing thousands of identical copies of CP (Figure 1a). In a surface area of 1 μm^2, VLPs can arrange 125 560 CPs. By cell lysis and ultracentrifugation in 25% sucrose gradient, VLPs can be purified from the host bacterial cells. Figure 1b shows the VLP nanorods with the lengths of 200 nm−1 μm after purification process. The maximum concentration of VLPs can reach 4 mg/mL in 0.1 M sodium phosphate buffer solution (pH = 7). The purified VLPs can be diluted using 0.1 M sodium phosphate buffer down to 0.2 mg/mL but still ensure effective assembly on gold surfaces.[22,23,25,26] The dependency between antibody-sensing efficacy and VLP concentrations (0.2, 2, or 4 mg/mL) utilized in sensor functionalization processes will be analyzed. All chemicals used in buffer preparation were obtained from Fisher Scientific, Waltham, MA. The solutions are based on deionized (DI) water (resistivity equals 18 MΩ·cm) from an E-Pure ultrapure water purification system. The genetic modifications, culture of the bacterial host, and purification procedures of VLPs were reported in detail previously.[19] The functionalities of VLP-FLAG as a bionanoreceptor come from the expressions of a receptor peptide epitope and a cysteine residue on each CP (Figure 1c). The FLAG-tag peptide (DYKDDDDK) showing high affinity to the target anti-FLAG antibody is expressed on the C-terminus of the VLP CP. On the N-
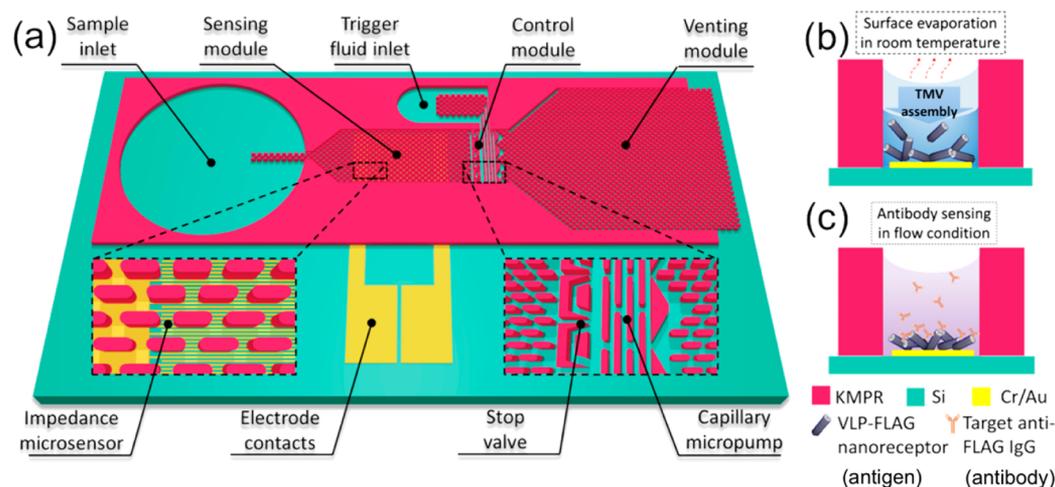
Figure 2. (a) 3D schematic showing the design of the sensor microsystem composed of open-channel capillary microfluidics and impedance sensor. The exploded views show (left) interdigitated electrode of the impedance sensor in the sensing module and (right) the details of the stop valve and triggering channel designs in the control module. Cross-sectional schematics show the experimental procedure for (b) VLP-FLAG (genetically expressing peptide antigen sequence) surface functionalization and (c) target anti-FLAG antibody sensing in capillary microfluidics.
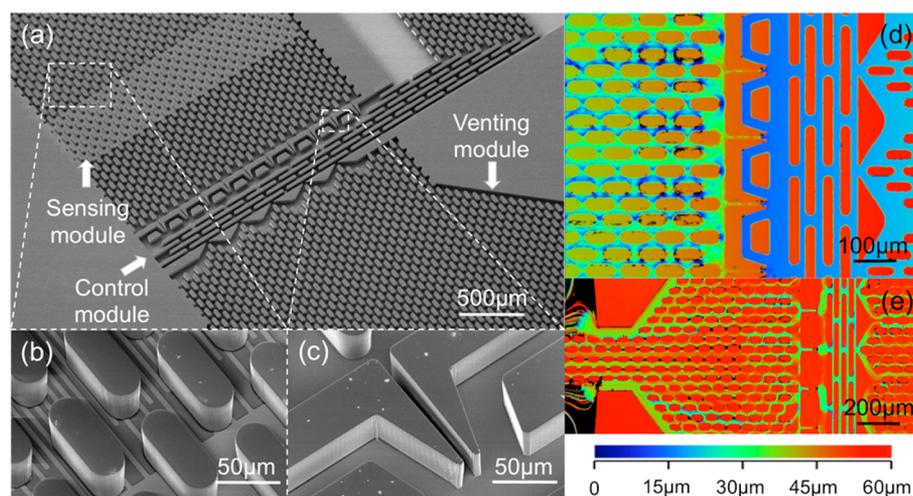

Figure 3. Scanning electron microscopy (SEM) images show (a) the overview of the microfabricated sensing microsystem containing sensing, control and venting module, (b) the interdigitated electrodes of the impedance sensor in the sensing module, and (c) the capillary stop valve in the control module. Optical profilometry images show (d) liquid sample filling in the sensing module before triggering of stop valves and (e) trajectories of microbeads in the capillary microfluidic subsystem after the triggering of stop valves.

terminus of each VLP CP, a cysteine residue is expressed to promote the binding between VLP nanoreceptors and gold impedance sensor electrodes via its thiol group. A different construct of the VLP (VLP-1cys), which shares the similar nanorod structure of VLP-FLAG but in the absence of FLAG-tag peptides, is utilized in the control experiments.

Open-Channel Capillary Microfluidics and Sensor Platform. The integrated sensing microsystem is composed of capillary microfluidics and an impedance sensor, aiming at autonomous liquid sample delivery, receptor localization, accelerated sensor functionalization, and real-time label-free sensing of target molecules. Figure 2a shows the schematic of the integrated sensing microsystem. According to the different functions, the system components can be catalogued into three essential modules: sensing, control, and venting. An impedance sensor and a capillary micropump comprise the sensing module. The impedance sensor spans a 2 mm × 2 mm area with interdigitated electrodes of 4 μm width and spacing. Capillary microfluidic subsystem uses capillary action and surface energy changes to manipulate the flow of liquid samples in a microfluidic channel[27−29] and has recently been exploited as an autonomous liquid sample delivery component in biosensors.[30,31] Here, the capillary microfluidic system utilizes open-channel capillary pumps (arrays of rounded rectangular pillars) and stop valves (sharp nozzles) to achieve rapid, controlled and localized VLP nanoreceptor assembly on an impedance sensor. The localization of VLPs is realized by autonomous delivery of the VLP-containing buffer solution onto the sensor electrode surface and confinement using capillary stop valves. The capillary micropump in the sensing module can autonomously deliver the VLP-containing solution onto the impedance sensor through capillary action. Owing to a large micropump area and open top surface, the VLP-containing solution will be rapidly evaporated from at the micropump area. This will contribute to inhanved attachment of VLPs to the impedance sensor surface through both thiol-gold interactions and van der Waals forces. The control module contains capillary stop valves and a triggering micropump with the channel direction perpendicular to the sensing and venting micropumps. The theoretical analysis of capillary microfluidic channel and principle of operation of the sensing microsystem is included in the Supporting Information.

During sensor functionalization with VLPs, 5 μL of 0.1 M sodium phosphate buffer solution containing VLPs at concentrations of 0.2, 2, or 4 mg/mL were pipetted in the sample inlet. Because of capillary
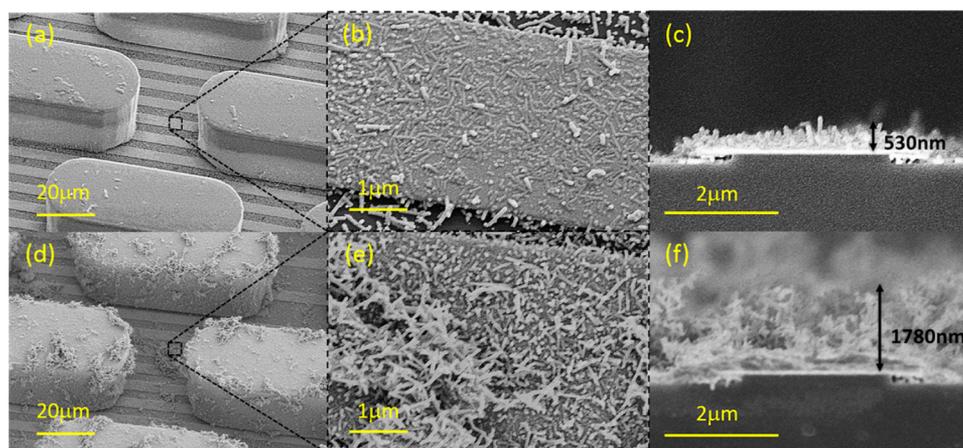
Figure 4. SEM images of the VLP-FLAG functional nanoreceptor layer assembled through autonomous delivery and enhanced evaporation in the open-channel capillary microfluidics. The morphology of VLP nanoreceptors assembled using (a) 0.2 mg/mL VLP-FLAG in 0.1 M phosphate buffer, where the enlarged view (b) and cross-sectional view (c) show the VLP nanorod assembled in parallel with the impedance sensor surface, forming a flat arrangement of nanoreceptors. The morphology of VLP nanoreceptors assembled (d) 4 mg/mL VLP-FLAG in 0.1 M phosphate buffer, where the enlarged view (e) and cross-sectional view (f) show the VLP nanorods form clusters and piled up on the impedance sensor electrode due to van der Waals force or electrostatic interactions.

action, the VLP solution was automatically distributed on the impedance sensor surface. The stop valves confine the VLP solution to the left sensing module due to the local energy barrier induced by the sharp change in the sidewall geometry. The VLP concentration above the impedance sensor increased as the solution evaporated, promoting high-density assembly of VLPs on the sensor through both thiol−gold binding and van der Waals forces (Figure 2b).

During antibody sensing, 1 μL of 1X Tris-buffered saline (TBS) was introduced from the triggering channel after the antibody-containing buffer solution filled the entire sensing module, which broke the barrier of the stop valves and induced continuous flow of test samples from the sensing to the venting module (Figure 2c). The sensor was first rinsed twice with 5 μL of 1X TBS solution to remove nonspecifically attached VLPs from the sensor surface. Then, the target anti-FLAG antibodies with increasing concentration from 10 ng/mL to 100 μg/mL in 5 μL of 1X Tris buffer were added from the sample inlet. The electrical impedance on the sensor was measured in real time during both VLP sensor functionalization and target antibody binding. Specifically, an AC signal at 100 Hz with amplitude of 50 mV was applied between the IDT electrodes using a VSP-300 potentiostat (Bio-Logic Science Instruments SAS, France) to analyze the VLP assembly dynamics and quantify the target molecule concentration.

RESULTS AND DISCUSSION

Capillary Microfluidics Fabrication and Characterization. The surface morphology of the microfabricated sensing system was characterized using scanning electron microscopy (SEM) and optical interferometry. Figures 3a−c are the SEM images showing the fabricated capillary stop valves and the micropumps in the sensing and triggering modules. The KMPR 1050 negative photoresist shows high-aspect-ratio pillar structures with smooth sidewalls. KMPR micropillars show good adhesion on the impedance sensor IDT electrode area (Figure 3b). The stop valves change the initial liquid meniscus−sidewall angle to more than 150°, forming sharp nozzle shapes and a localized free energy barrier (Figure 3c). Optical profilometry was utilized to further inspect the geometric dimensions of the microfluidic layer. The depth of each channel in the capillary micropump is measured as 60 μm (Figure S6), while the minimum channel width is 15 μm at the stop valves. A 5 min O$_2$ plasma treatment was performed on

the KMPR microfluidic layer surface to render the microfluidic sidewalls hydrophilic with the contact angle of 6° (Figure S7).

The flow regulation function of the stop valves before triggering, and the flow distribution in the system after the triggering of stop valves, were characterized using optical interferometry. A 5 μL water sample containing polystyrene microbeads of 10 μm diameter were loaded from the sample inlet. These microbeads were confined in the sensing module due to the presence of capillary stop valves. The movements of the microbeads due to the initial filling in the channel and the Brownian motion distorted the water/air interface, creating a different reflection patterns compared with water. The trajectories of these microbeads were recorded using vertical scanning interferometry in optical profilometry operating at a low scan rate of 1 μm/s. The optical profilometry image in Figure 3d shows that the microbeads suspended in DI water were confined only in the sensing modules on the left of the stop valves, leaving both triggering and venting modules unfilled. This reflects the circumstances present when the VLP-containing solution is introduced during the sensor functionalization process. Figure 3e demonstrates the distribution of flow in the microsystem after triggering of the stop valves. The liquid sample that contains polystyrene microbeads flew through the sensing module and left an evenly distributed trajectory pattern of the microbeads. This even distribution enabled the delivery of target molecules on the full area of the sensor and thus maximize the use of assembled VLPs toward sensitive antibody detection. Further flow distribution analysis using the image tool ImageJ is available in the Supporting Information.

VLP Assembly in Capillary Microfluidics. The surface morphology of the VLP nanoreceptor assembled through evaporation in the capillary microfluidic device was studied using scanning electron microscopy (SEM). Palladium activation and electroless nickel coating were performed on the VLP-assembled device to enhance the SEM imaging contrast. Figure 4a shows the uniform coating of VLP-FLAG nanoreceptors on the impedance sensor IDT electrodes and the sidewall of the microfluidic channel using 0.2 mg/mL VLPs in the buffer solution. The enlarged view in Figure 4b shows flat

and dense attachment of VLP-FLAG nanoreceptors on the IDT electrode surface, forming a thin VLP functional layer. When the concentration of VLPs is increased to 4 mg/mL, the VLPs form clusters due to the nonspecific binding caused by van der Waals forces and electrostatic interactions (Figure 4d). These clusters of VLP nanoreceptors increase the total volume of VLPs available in the sensor system; however, a closer view of the VLP morphology on the electrode also shows that the high concentration VLPs result in the aggregation of these nanoreceptors with random orientation (Figure 4e). Overall, with both low and high VLP concentrations, the density of the assembled VLPs on the impedance sensor through evaporation in the open capillary microfluidics is much higher compared to that previously achieved in a closed chamber.[31] The cross-sectional SEM images of the VLP-assembled sensor electrode show distinct difference in the VLP layer when difference VLP concentrations are utilized in the assembly process. A low VLP concentration (0.2 mg/mL) resulted in a low VLP layer thickness of 0.53 μm (Figure 4c). And, a high VLP concentration (4 mg/mL) in the assembly process formed a thick VLP layer of 1.78 μm (Figure 4f, more than 3-fold of that achieves using a lower VLP concentration).

Figure 5a shows the original SEM images and the processed images of the VLP-FLAGs assembled on gold impedance
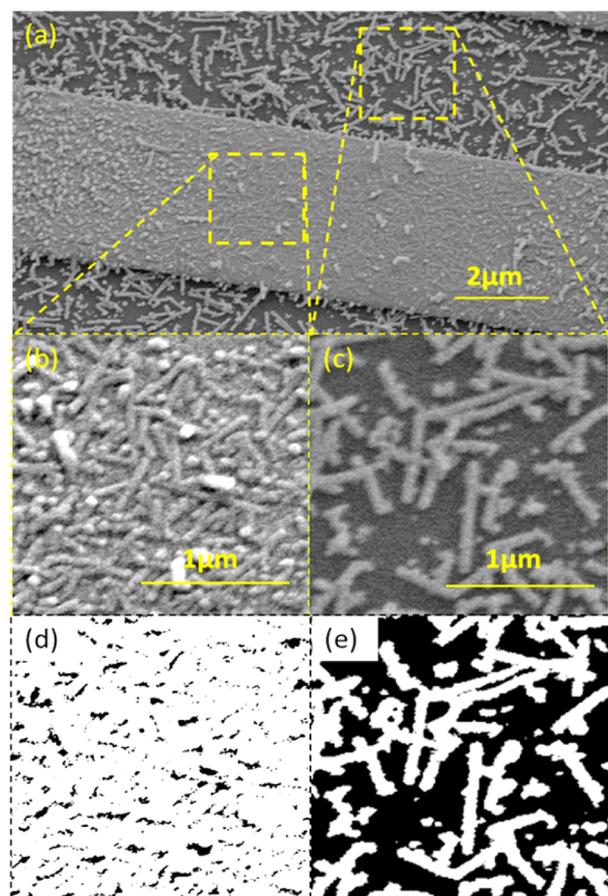

Figure 5. Analysis of VLP-FLAG assembly coverage on gold (specific binding) and silicon (nonspecific binding) using scanning electron microscopy images and the image processing tool ImageJ. SEM images of (a) VLP-assembled gold and silicon surfaces, (b) VLP on gold, and (c) VLP on silicon. (d) and (e) are processed binary images from (b) and (c), respectively.

electrode and silicon surfaces. The zoom-in pictures (Figure 5b,c) show that significantly larger numbers of VLP rods assembled on the gold surface compared to the silicon surface. This validated the effect of covalent binding between the gold and thiol groups on the cysteine modified VLPs. To further analyze the nonspecific assembly of VLPs on silicon surface, the original SEM images (Figure 5b,c) with 4 μm^2 total area were processed using the image processing software ImageJ. The original images were first processed through proper threshold value setting, which marks the dark areas that were not covered by any VLPs. Then the images were converted into binary images where the white color represents VLP and the black color represents uncovered areas (Figure 5d,e). The VLP coverage can then be calculated using the average gray value of each image. Table 1 summarizes the average gray values and

Table 1. Analysis of VLP Coverage on Gold and Silicon through Image Processing

surface material	image source	average gray value (1–255)	calculated VLP assembly coverage (%)
gold (specific assembly)	Figure 5d	232	91
silicon (nonspecific assembly)	Figure 5e	105	41

calculated VLP coverage from analyzing the images of Figure 5d,e. In the image analysis, all the pixels of Figure 5d,e have been counted in evaluation of the average gray values. The specific VLP assembly on gold reaches 91% while the nonspecific assembly of VLP on silicon is 41%. The nonspecific assembly of VLP may result from van der Waals force during evaporation-assisted assembly process.

Real-Time and Label-Free Antibody Sensing Using VLP-Functionalized Impedance Sensor. The electrical impedance between the interdigitated electrodes was measured every 10 s during both VLP assembly on-chip and antibody sensing. The percentage impedance change (imaginary part of the complex impedance) at 100 Hz was utilized to analyze the VLP and antibody attachments on the electrode surface. When biological particles (relative permittivity of 4–13) attach to the electrode surface, they displace water (relative permittivity of ~80) on the electrode/liquid interface. This lowers the effective dielectric constant on the electrode surface and reduces the area (and thus the associated capacitance) of the ionic double layer defined by the electrode/electrolyte interface. Therefore, an increase in the amplitude of impedance (imaginary part) is expected as biomolecules attach to the electrodes.

Figure 6a shows the evolution of the relative impedance during the assembly of VLP on the sensor's IDT electrodes. It is shown that using the open capillary microfluidic device as delivery platform, the impedance between the IDT electrodes increased by more than 120% and saturated within 6 min after introducing a drop of 0.2 mg/mL VLP-FLAG nanoreceptors. In contrast during the control experiment, the impedance changed less than 2% when only buffer solution was delivered. In previous work that utilized VLP self-assembly, the VLP could saturate the electrode surfaces in 18 h. The accelerated VLP assembly process using the capillary microfluidic system may be due to the local increase in VLP concentration as buffer evaporates and more solution is drawn in via the capillary pump. These results show not only the capability of using
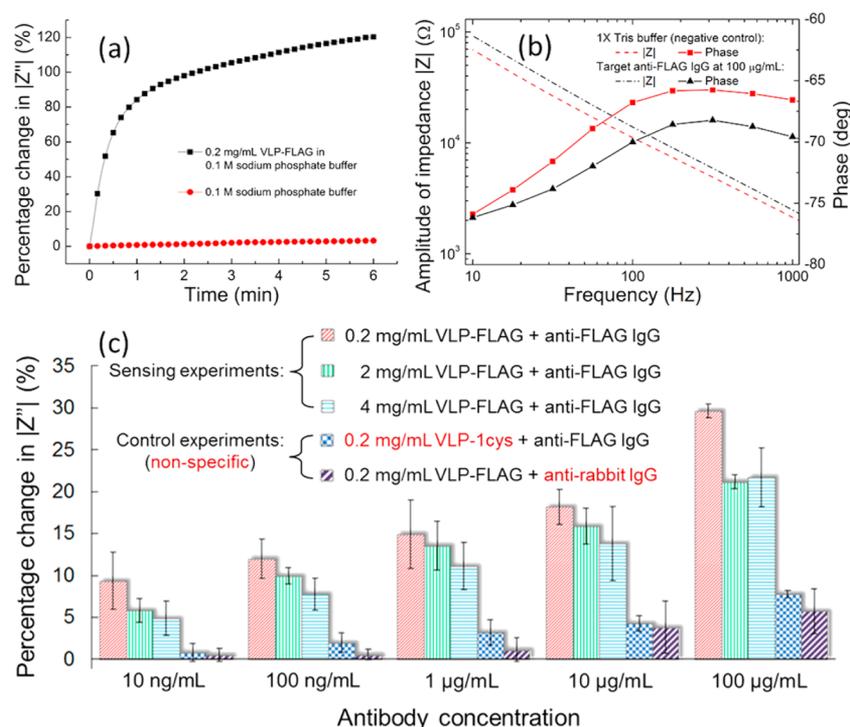
Figure 6. (a) Real-time percentage changes in the impedance (amplitude of imaginary part) between IDT electrodes during VLP assembly. (b) Impedance magnitude and phase responses of the sensor to TBS buffer and antibody targets in TBS buffer. (c) Percentage impedance changes when antibodies were introduced to the VLP-functionalized impedance sensors. Complementary receptors and targets—VLP-FLAG and anti-FLAG IgG—were utilized in the sensing experiments. In the two control experiments, nonspecific receptors (VLP-1cys at 0.2 mg/mL) or nonspecific target antibodies (anti-rabbit IgG) were used. Experiments with the same conditions have been repeated independently on multiple sensors ($n = 3$). The error bars represent the standard deviations.

impedance sensors in studying the dynamics of nanoreceptor assembly on sensors but the great advantage of using open-channel capillary microfluidics to accelerate the assembly process through enhanced evaporation as well.

After the accelerated VLP assembly, the target anti-FLAG with increasing concentrations was sequentially applied onto the VLP-functionalized impedance sensors surfaces. Compared to negative control experiment using Tris buffer, the impedance amplitude of VLP-functionalized microsensor showed clear increase after exposing to the target anti-FLAG IgG at the concentration of 100 μg/mL. At 100 Hz, the decrease in the phase (>3.2°) further validated that the increase in impedance amplitude is majorly resulted from a lower capacitance from biological targets binding (Figure 6b). Figure 6c shows the resulting percentage change in imaginary impedance of the VLP-functionalized sensors. Impedance shifts from nonspecific bindings were studied in two control experiments. In the first control experiment, nonspecific VLP-1cys nanorods at 0.2 mg/mL concentration were used to functionalize the sensors, which generated the impedance changes of less than 7.8% at the maximum anti-FLAG concentration of 100 μg/mL. In the second control experiment, the sensors functionalized by VLP-FLAG at 0.2 mg/mL responded to nonspecific binding anti-rabbit IgG with the maximum of 5.7% impedance changes. On the other hand, the impedance sensors functionalized using VLP-FLAGs at various concentrations all showed significantly larger impedance increases. This indicates that VLP-FLAG is a highly selective biosensing probe with respect to the target antibody. Interestingly, when the impedance sensor was functionalized using the lowest concentration of VLP-FLAG (0.2 mg/mL), the highest sensitivity during antibody binding

was observed (real-time impedance responses are available in the Supporting Information). At the maximum target antibody concentration of 100 μg/mL, the impedance sensor functionalized using 0.2 mg/mL VLP-FLAG showed an impedance increase of 29.6% while the one functionalized using 4 mg/mL VLP-FLAG only showed an increase of 21.2%. This substantial difference in the sensor performance may be a result of the significant difference in the VLP morphology achieved by using different VLP concentrations during assembly. A higher VLP concentration leads to a thicker VLP layer, which kept the subsequently attached antibodies away from the electrode surface, thereby decreasing the sensor sensitivity. Using a lower VLP concentration, the VLPs assembled as a closely packed flat monolayer on the electrode surface, allowing the attached antibodies to directly impact the double layer capacitance, thus increasing the sensitivity of the system. Therefore, among all the tested VLP concentrations (0.2, 2, and 4 mg/mL), the 0.2 mg/mL is the most favorable sensor functionalization condition to achieve a better antibody sensing. The maximum sensitivity calculated from Figure 6c is 4.12% impedance change per log(ng/mL) antibody concentration. The error bars in Figure 6c were calculated from the standard deviations of three independent experiments for each experiment condition using new sensors. The resolution of the VLP-functionalized sensors was calculated to be 3.9% impedance change (3 times the standard deviation when measuring buffer solution (negative control)). Therefore, the detection limit of the VLP-FLAG functionalized sensor is 8.84 ng/mL (equivalent to 55 pM anti-FLAG IgG). The results showed great potential of using VLP-functionalized impedance sensors to perform rapid label-free biosensing in real time.
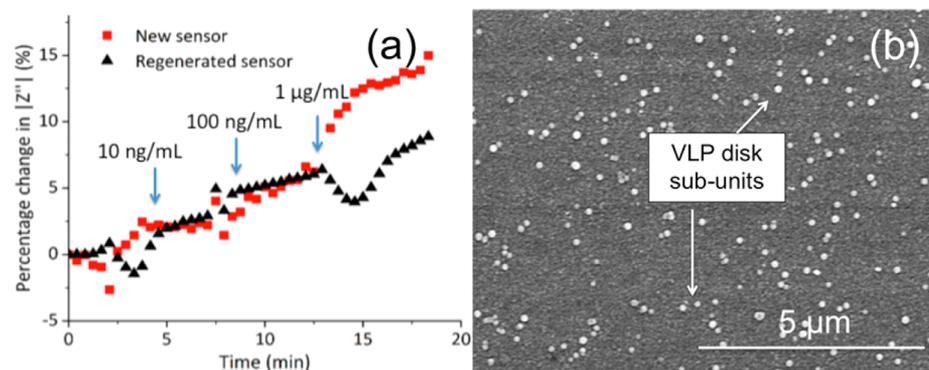
Figure 7. (a) Impedance responses to increasing target anti-FLAG concentration on a sensor before and after surface regeneration. (b) SEM image showing the morphology of the metalized VLP-coated surfaces after cleaning with 2% NaOH cleaning at room temperature. The white dots are VLP disk-like subunit residues on the gold surface.

Sensor Regeneration. In the experiments, we have flushed the microfluidic devices with 5 μL of 2% NaOH solution for 5 min for sensor regeneration. In our previous work, it has been demonstrated that the rodlike VLP coat protein structure responses to base solution (pH > 7) and disassembles from rod to disk subunits.[19] Therefore, using NaOH solution to wash the VLP-based sensor surface can cause VLP disassembly and regenerate sensor surface. The impedance responses from the same sensor before and after surface regeneration are compared in Figure 7a. With either new sensor or regenerated sensor, the impedance responses were similar to the increasing target antibody concentration from 10 ng/mL to 1 μg/mL, and the maximum impedance increase was of around 7%. However, the new sensor showed more stable and continuous impedance increase compared with the regenerated sensor. However, as the antibody concentration increased further to 1 μg/mL, the new sensor showed higher impedance change of 15% compared with lower than 10% from the reused sensor. We have investigated the VLP-assembled gold surface after washing with 2% NaOH using SEM imaging. The SEM image in Figure 7b shows that over 95% of the gold previously assembled with VLPs has been cleaned using NaOH solution, and around 5% of the area is still covered by VLP disklike subunits (white round particles on the SEM image). The impedance fluctuation in the regenerated sensor may attribute to the detachment of VLPs on the surface due to degraded VLP binding strength on the surface. The new sensor also showed slightly larger impedance increase compared with the regenerated one. Though there are differences in the sensor characteristics due to the regeneration, the VLP-functionalized regenerated sensor can still be utilized to perform label-free antibody sensing and quantify the concentration of the target molecule. Therefore, NaOH wash in the integrated sensor system can serve as a viable means to make most of the VLP-based receptors detach from the sensor surface without sacrificing the device integrity.

In our previous work, we have also tested the FLAG-tag modified VLPs and anti-FLAG IgG binding in the human whole blood using impedimetric sensor with the limit of detection down to 150 nM.[33] Our published work validated that the blood or serum sample will not degrade the VLP binding affinity to the target antibodies, nor will the media cause disassembly of VLPs from the sensor surface. Therefore, we believe, by modifying our current capillary microfluidic device design to include additional sample preparation units such as blood filter, the system will be suitable for detection of antibodies in the blood sample. At the current stage, we are

more focused on using preprocessed pure sample and buffer solution to characterize the VLP-based sensor performance.

◼ CONCLUSION

In summary, an integrated microsystem was developed and tailored toward accelerated, enhanced, and controlled microsensor surface functionalization with TMV VLP bionanoreceptors. A capillary microfluidic system composing passive micropumps and stop valves was utilized as preprogramed and autonomous mechanisms to achieve rapid, dense, and localized nanoreceptor assembly on the sensor. An impedance sensor was integrated on the platform to study the dynamics of biological sensing probe assembly on the sensor surface and monitor the impedimetric responses during antibody−antigen binding events in real time. The impedance change showed that utilizing the developed open-channel capillary microfluidics, the VLP sensing probe can be rapidly assembled on the sensor as a biorecognition layer within 6 min, a significant reduction in time compared with the previous 18 h process.[32] The functionalized sensor was capable of label-free sensing of the target antibodies in 5 min with the detection limit of 55 pM. To the best of our knowledge, it is the first time that open-channel microfluidic devices are utilized to autonomously manipulate the biological nanoreceptor distribution and create a functional interface on the transducer surface. This lead to 180× faster VLP assembly time, 200× smaller VLP sample volume, and 1.5× higher coverage on the electrode compared to our previous work.[32] Also, the improvement in receptor layer eventually leads to higher sensitivity and contributed to label-free antibody sensing that can only be achieved using full immunoassay with labeling.[32] We believe that by combining genetic modification of TMV-VLP and microfluidic-assisted assembly method, the TMV-VLPs can be utilized as fast and programmable bioreceptors in fast-response biosensing applications

This work leveraged the genetic modification capabilities of the VLP bionanoreceptors and the controllability of the microsystem for rapid, on-demand, and label-free biosensing. It provided a system-level solution to improve both the efficiency and quality in sensor functionalization through (1) expression of high-density binding peptides in the molecular scale ($\sim$1.26 × 10^5 binding peptides per μm^2, assuming a full exposure of VLP peptides) and (2) creation of densely arranged macromolecules in the system scale (91% surface coverage). It has shown the great potential of using VLP receptors and microsystems to create versatile, decentralized,

and on-demand biosensors for both applications in public and personal health.

ASSOCIATED CONTENT

ⓢ Supporting Information

The Supporting Information is available free of charge on the ACS Publications website at DOI: 10.1021/acsami.6b14045.

> VLP genetic modification, capillary microfluidic system design and operation principles, device microfabrication and surface treatment procedures, optical profilometry analysis of fabricated devices and flow distribution, real-time impedance response during VLP−antibody binding (PDF)
>
> Video showing the operation of capillary microfluidic pump and stop valve array (MPG)
>
> Notes for video (PDF)

AUTHOR INFORMATION

Corresponding Author

*E-mail: ghodssi@umd.edu (R.G.).

ORCID ⓘ

Faheng Zang: 0000-0002-1173-6553

Notes

The authors declare no competing financial interest.

ACKNOWLEDGMENTS

REFERENCES

(1) Mangili, A.; Gendreau, M. A. Transmission of Infectious Diseases during Commercial Air Travel. *Lancet* **2005**, *365* (9463), 989−996.

(2) Taubenberger, J. K.; Morens, D. M. The Pathology of Influenza Virus Infections. *Annu. Rev. Pathol.: Mech. Dis.* **2008**, *3*, 499−522.

(3) Colizza, V.; Barrat, A.; Barthelemy, M.; Vespignani, A. The Role of the Airline Transportation Network in the Prediction and Predictability of Global Epidemics. *Proc. Natl. Acad. Sci. U. S. A.* **2006**, *103* (7), 2015−2020.

(4) Teles, F. S. R. R. Biosensors and Rapid Diagnostic Tests on the Frontier between Analytical and Clinical Chemistry for Biomolecular Diagnosis of Dengue Disease: A Review. *Anal. Chim. Acta* **2011**, *687* (1), 28−42.

(5) Urban, G.; Jobst, G.; Kohl, F.; Jachimowicz, A.; Olcaytug, F.; Tilado, O.; Goiser, P.; Nauer, G.; Pittner, F.; Schalkhammer, T.; Mannbuxbaum, E. Miniaturized Thin-Film Biosensors using Covalently Immobilized Glucose-Oxidase. *Biosens. Bioelectron.* **1991**, *6* (7), 555−562.

(6) Belkin, S. Microbial Whole-cell Sensing Systems of Environmental Pollutants. *Curr. Opin. Microbiol.* **2003**, *6* (3), 206−212.

(7) Wang, J. Amperometric Biosensors for Clinical and Therapeutic Drug Monitoring: A Review. *J. Pharm. Biomed. Anal.* **1999**, *19* (1−2), 47−53.

(8) Chin, C. D.; Linder, V.; Sia, S. K. Lab-on-a-chip Devices for Global Health: Past Studies and Future Opportunities. *Lab Chip* **2007**, *7* (1), 41−57.

(9) Wang, S. Q.; Thomas, A.; Lee, E.; Yang, S.; Cheng, X. H.; Liu, Y. L. Highly Efficient and Selective Isolation of Rare Tumor Cells using a Microfluidic Chip with Wavy-herringbone Micro-patterned Surfaces. *Analyst* **2016**, *141* (7), 2228−2237.

(10) Su, L. A.; Jia, W. Z.; Hou, C. J.; Lei, Y. Microbial Biosensors: A Review. *Biosens. Bioelectron.* **2011**, *26* (5), 1788−1799.

(11) Lei, Y.; Chen, W.; Mulchandani, A. Microbial biosensors. *Anal. Chim. Acta* **2006**, *568* (1−2), 200−210.

(12) Mao, C. B.; Liu, A. H.; Cao, B. R. Virus-Based Chemical and Biological Sensing. *Angew. Chem., Int. Ed.* **2009**, *48* (37), 6790−6810.

(13) Lee, J. H.; Domaille, D. W.; Cha, J. N. Amplified Protein Detection and Identification through DNA-Conjugated M13 Bacteriophage. *ACS Nano* **2012**, *6* (6), 5621−5626.

(14) Olsen, E. V.; Sorokulova, I. B.; Petrenko, V. A.; Chen, I. H.; Barbaree, J. M.; Vodyanoy, V. J. Affinity-selected Filamentous Bacteriophage as a Probe for Acoustic Wave Biodetectors of Salmonella Typhimurium. *Biosens. Bioelectron.* **2006**, *21* (8), 1434−1442.

(15) Hayat, A.; Andreescu, S.; Marty, J. L. Design of PEG-aptamer two piece macromolecules as convenient and integrated sensing platform: Application to the Label Free Detection of Small Size Molecules. *Biosens. Bioelectron.* **2013**, *45*, 168−173.

(16) Boozer, C.; Ladd, J.; Chen, S. F.; Jiang, S. T. DNA-directed Protein Immobilization for Simultaneous Detection of Multiple Analytes by Surface Plasmon Resonance Biosensor. *Anal. Chem.* **2006**, *78* (5), 1515−1519.

(17) Culver, J. N.; Brown, A. D.; Zang, F. H.; Gnerlich, M.; Gerasopoulos, K.; Ghodssi, R. Plant Virus Directed Fabrication of Nanoscale Materials and Devices. *Virology* **2015**, *479*, 200−212.

(18) Fan, X. Z.; Pomerantseva, E.; Gnerlich, M.; Brown, A.; Gerasopoulos, K.; McCarthy, M.; Culver, J.; Ghodssi, R. Tobacco Mosaic Virus: A Biological Building Block for Micro/nano/bio systems. *J. Vac. Sci. Technol., A* **2013**, *31* (5), 050815.

(19) Brown, A. D.; Naves, L.; Wang, X.; Ghodssi, R.; Culver, J. N. Carboxylate-Directed In Vivo Assembly of Virus-like Nanorods and Tubes for the Display of Functional Peptides and Residues. *Biomacromolecules* **2013**, *14* (9), 3123−3129.

(20) Chiang, C. Y.; Epstein, J.; Brown, A.; Munday, J. N.; Culver, J. N.; Ehrman, S. Biological Templates for Antireflective Current Collectors for Photoelectrochemical Cell Applications. *Nano Lett.* **2012**, *12* (11), 6005−6011.

(21) Yi, H. M.; Nisar, S.; Lee, S. Y.; Powers, M. A.; Bentley, W. E.; Payne, G. F.; Ghodssi, R.; Rubloff, G. W.; Harris, M. T.; Culver, J. N. Patterned Assembly of Genetically Modified Viral Nanotemplates via Nucleic Acid Hybridization. *Nano Lett.* **2005**, *5* (10), 1931−1936.

(22) Zang, F.; Gerasopoulos, K.; Fan, X. Z.; Brown, A. D.; Culver, J. N.; Ghodssi, R. An Electrochemical Sensor for Selective TNT Sensing Based on Tobacco Mosaic Virus-like Particle Binding Agents. *Chem. Commun.* **2014**, *50* (85), 12977−12980.

(23) Zang, F.; Fan, X. Z.; Gerasopoulos, K. D.; Ben-Yoav, H.; Brown, A. D.; Culver, J. N.; Ghodssi, R. *Scale-down Effects: Towards Miniaturization of an Electrochemical Sensor using Biomolecules, SENSORS, 2013 IEEE, Baltimore, USA*; IEEE: Baltimore, MD, 2013; pp 1−4.

(24) Zang, F.; Gerasopoulos, K.; McKinzie, K.; Culver, J.; Ghodssi, R. *Autonomous Capillary Microfluidics for Rapid Nanoreceptor Assembly and Biosensing, Solid-State Sensors, Actuators and Microsystems (TRANS-DUCERS), 2015 Transducers-2015 18th International Conference on, Anchorage, USA*; IEEE: Anchorage, AK, 2015; pp 548−551.

(25) Gnerlich, M.; Pomerantseva, E.; Gregorczyk, K.; Ketchum, D.; Rubloff, G.; Ghodssi, R. Solid Flexible Electrochemical Supercapacitor using Tobacco Mosaic Virus Nanostructures and ALD Ruthenium Oxide. *J. Micromech. Microeng.* **2013**, *23* (11), 114014.

(26) Gerasopoulos, K.; Pomerantseva, E.; McCarthy, M.; Brown, A.; Wang, C. S.; Culver, J.; Ghodssi, R. Hierarchical Three-Dimensional Microbattery Electrodes Combining Bottom-Up Self-Assembly and Top-Down Micromachining. *ACS Nano* **2012**, *6* (7), 6422−6432.

(27) Laser, D. J.; Santiago, J. G. A Review of Micropumps. *J. Micromech. Microeng.* **2004**, *14* (6), R35−R64.

(28) Zimmermann, M.; Schmid, H.; Hunziker, P.; Delamarche, E. Capillary Pumps for Autonomous Capillary Systems. *Lab Chip* **2007**, *7* (1), 119−125.

(29) Zimmermann, M.; Hunziker, P.; Delamarche, E. Valves for Autonomous Capillary Systems. *Microfluid. Nanofluid.* **2008**, *5* (3), 395−402.

(30) Gervais, L.; Delamarche, E. Toward One-step Point-of-care Immunodiagnostics using Capillary-driven Microfluidics and PDMS Substrates. *Lab Chip* **2009**, *9* (23), 3330−3337.

(31) Hitzbleck, M.; Gervais, L.; Delamarche, E. Controlled Release of Reagents in Capillary-driven Microfluidics using Reagent Integrators. *Lab Chip* **2011**, *11* (16), 2680−2685.

(32) Zang, F.; Gerasopoulos, K.; Fan, X. Z.; Brown, A. D.; Culver, J. N.; Ghodssi, R. Real-time Monitoring of Macromolecular Biosensing Probe Self-assembly and On-chip ELISA using Impedimetric Microsensors. *Biosens. Bioelectron.* **2016**, *81*, 401−407.

(33) Winkler, T.; Zang, F.; Stevenson, F.; Culver, J.; Ghodssi, R. Portable Immunoassay for Label-Free Antibody Detection in Whole Blood. Technical Digest of International Conference on Miniaturized Systems for Chemistry and Life Sciences (μTAS) Dublin, Ireland, 2016; pp 661−662.